Investigating excited electronic states of I_2^+ and I_2^{2+} produced by strong-field ionization using vibrational wave packets

L. Fang and G. N. Gibson
Department of Physics, University of Connecticut, Storrs, Connecticut 06269
(Received 6 February 2007; published 8 June 2007)

In pump-probe experiments with a femtosecond near-uv laser, a wave packet is launched onto an excited electronic state of I_2^+ through strong field ionization, and starts vibrating in the corresponding potential well. The vibrational wave packet is further ionized by a probe pulse to an excited electronic state of I_2^{2+} that dissociates into $I^{2+}+I^{0+}$. Projecting the vibrational wave packet onto the dissociation channel reveals characteristics of both potential curves via the periodic variations in kinetic energy distribution of the dissociating fragments. The experimental results are consistent with theoretical simulations that are sensitive to the shape of the potential curves. We find that the intermediate state in I_2^+ is $A^2\Pi_{u,3/2}$ and ionization to this state has an anomalous angular dependence. Moreover, we extract the $I^{2+}+I^{0+}$ potential energy curve and find evidence for a truly bound potential well, in contrast to the metastable ground state potential energy curves.

DOI: 10.1103/PhysRevA.75.063410 PACS number(s): 33.80.Rv, 32.80.Rm, 42.50.Hz

I. INTRODUCTION

Neutral I_2 has been well studied both experimentally and theoretically [1–3]. However, certain aspects of molecular ions and the electronic excited states correlating with charge asymmetric dissociation are poorly understood [4,5]. Moreover, excitation of I_2^+ through ionization is detrimental to the study of quantum tomography as this technique relies on the assumption that all ionization leaves the ion in its ground state [6,7].

Although there have been many studies on the strong field ionization of molecules with ion time-of-flight (TOF) spectroscopy, these experiments have generally been insensitive to excitation of the molecular ion. TOF data from pump-probe experiments have been used to identify dissociating excited electronic states [5], but did not determine whether bound molecular ions are electronically excited. Electron spectroscopy has been used to identify inner-orbital ionization in N_2 that leaves the ion in an electronically excited state [8], but this technique cannot measure characteristics of the excited state potential energy curves (PEC) or the angular dependence. This paper presents the work of identifying bound, electronically excited states of molecular ions in TOF using frequency analysis of the motion of wave packets induced in the potential wells. The motion of the wave packet is also used to investigate a dissociating curve of the doubly charged molecular ion, for which a bound region is found. Finally, the excitation is determined to occur through inner-orbital ionization and an anomalous angular dependence is found for this ionization process.

This paper is organized into five sections. We first describe the physical scenario and the experiments including the pump-probe configuration and general data representation. Second, we present the experimental results and the analysis. Next, we show the agreement between the experimental results and theoretical simulations that confirm our initial hypothesis. Following the experimental and simulation results, we discuss the validity of our method, the properties of the physical system our results reveal and the remaining discrepancy between experimental results and simulations that brings out further questions. Finally, we give the conclusions of this work.

II. EXPERIMENT

A. Physical scenario and experimental realization

Strong laser fields can typically remove many electrons from a molecule. The resulting molecular ion dissociates and the kinetic energy release (KER) has been the subject of many studies [12–16]. In this paper, we first focus on the very first ionization step. As shown in Fig. 1, a short laser pulse (pump) ionizes I_2 to I_2^+. While it is generally assumed that the ion is left in its ground state, it could end up in an excited state, for example, $I_2^+A^2\Pi_{u,3/2}$. In order to investigate

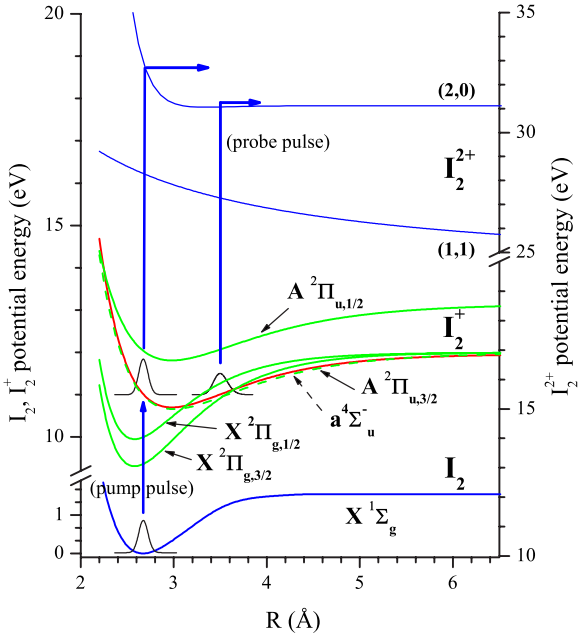

FIG. 1. (Color online) Schematic potential curves and physical scenario [1,9–11]. The minimum potential energy of the I_2 ground-state curve is used as the zero reference for all the curves plotted.

this possibility, we make use of the coherent evolution of the wave packet in the potential well of the ion. To image the motion of the wave packet, we use a second short pulse (probe) to further ionize it during its oscillation to an excited state of I_2^{2+} which dissociates into the asymmetric channel $I^{2+}+I^{0+}$, designated by (2,0) [5]. Since the kinetic energy that the dissociating fragments gain from the internuclear potential depends on the internuclear separation R where the dissociation is launched and the R is determined by the delay time between the two pulses (τ), the periodic distribution of KER detected as a function of delay time maps the vibrational motion of the wave packet; consequently, these data can be used to identify the corresponding state. Furthermore, since we can calculate the wave packet evolution of the $I_2^+ A^2\Pi_{u,3/2}$ state, we can use the KER as a function of τ to determine the (2,0) PEC.

B. Experimental setup

The work presented in this paper is performed with a home-built laser system consisting of a Kerr-lens mode locked Ti:Sapphire oscillator and a multipath Ti:Sapphire optical amplifier [17]. Short laser pulses from this system (~780 nm central wavelength, ~23 fs pulse width, 1 kHz repetition rate) are sent into a Michelson interferometer to produce identical pump and probe pulses. The pulse delay τ is varied by moving one of the retro mirrors controlled by a translation stage. The laser pulses are frequency doubled with a 250 μm-thick type-I beta barium borate (BBO) crystal in each arm of the interferometer. Polarizers and $\frac{1}{2}\lambda$ plates are used to control the polarization and the intensities of the pump and probe pulses independently. The two blue beams are recombined and dispersion compensated using a prism pair (to a pulse width of ~40 fs). The spatial overlap of the two beams is ensured by observing their foci after a converging lens on a charge-coupled device camera. Pulses are directed into a high-vacuum TOF mass spectrometer consisting of an extraction region and a drift region, and focused by a 3 inch-focal-length silver mirror inside the spectrometer chamber to ~8 μm diameter. I_2 gas is introduced into the chamber via a leak valve at pressures up to 1×10^{-5} torr above a base of 1×10^{-9} torr. TOF spectra are recorded by a pair of microchannel plates. The line that crosses the laser beam at a right angle and points directly to the detector is defined as the TOF axis (see Fig. 2). The basic experimental configuration is outlined in Ref. [18]. Zero time delay ($\tau=0$) is found by the enhanced signal of I_2^{3+} or H_2O^+ due to the increased laser intensity at $\tau=0$.

In TOF, the momentum of a dissociating channel is proportional to the difference in arrival time between the forward and backward going fragments. As shown in Fig. 2, only the projection of the momentum along the TOF axis can result in a difference in the arrival time. In our current work, the TOF spectrum is set to be symmetric with respect to the zero KER TOF. For dissociation along the TOF axis, the KER can be fully recorded and the dissociation channel produces two peaks symmetric with respect to the zero KER. Hence, the periodic variations in the KER as a function of τ will form a pair of symmetric wavelike tracks for increasing

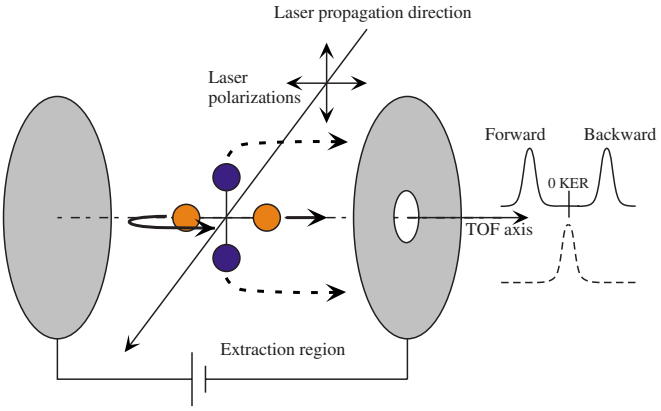

FIG. 2. (Color online) Schematic outline of the TOF spectrometer configuration showing dissociation along and transverse to the TOF axis and the corresponding TOF signals.

τ, which we call "loops" [see, for example, Fig. 3(a)]. For dissociation perpendicular to the TOF axis, the departing fragments will arrive at the detector at the same time, and the dissociation channel will produce a single peak centered at the zero KER point, similar to that for bound ions. However, in the extraction region of the spectrometer, there is a 1 mm pinhole on the exit plate. This pinhole controls the energy and angular acceptance of the spectrometer; only ions with low transverse KER are selected to pass through and be detected. Using classical ion trajectories, it is calculated that for dissociation perpendicular to the TOF axis those ions with a total KER of more than 0.75 eV will be blocked by the plate (denoted as angular blocking). Hence, in this case the disso-

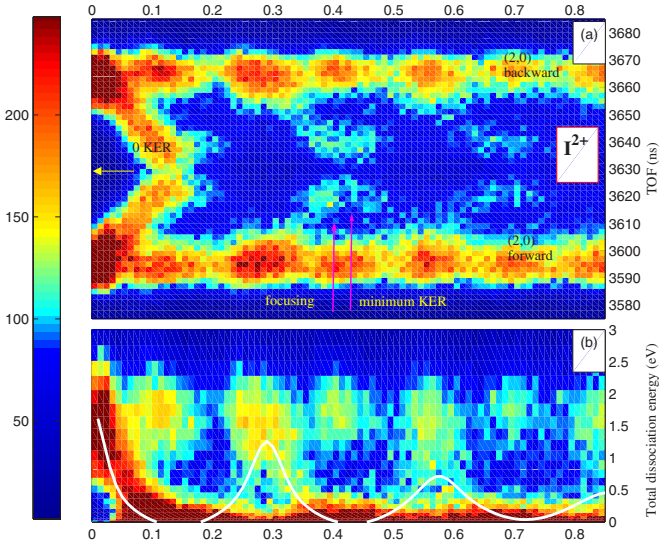

FIG. 3. (Color online) (a) TOF spectrum of I^{2+} versus τ with a step size of 0.010 ps. The pump pulse is perpendicular to the TOF axis and the probe pulse is parallel to the TOF axis. The periodic vibrations in KER form wavelike "loops." The pump pulse energy is 1.7 μJ giving estimated intensity of $\sim9\times10^{13}$ W/cm^2. The intensity ratio of the pump pulse to the probe pulse is 2:1. (b) Data of (2,0) channel (backward going) in (a) converted into KER space. Solid line: simulated vibrations in KER using the (2,0) curve obtained in our current work.

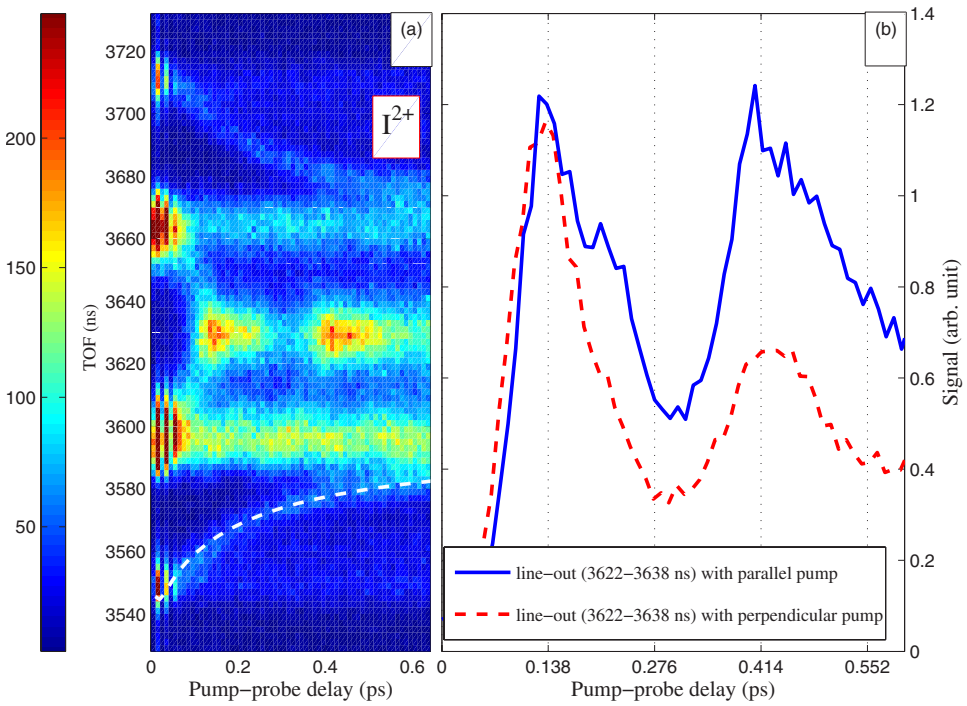

FIG. 4. (Color online) (a) TOF spectrum I^{2+} versus τ with a step size of 0.010 ps. The polarization of the pump and probe pulses are reversed compared with the data in Fig. 3. Vibrations in KER appear as "islands." The pump pulse energy is 0.9 μJ giving estimated intensity of $\sim 4.5\times 10^{13}$ W/cm^2. The intensity ratio of the pump to the probe is 1:2. Dashed line: $(2,0)\rightarrow(2,1)$ track simulated. (b) Solid line: line out of data in (a) of this figure. Dashed line: line out of data in Fig. 3(a).

ciation can only be detected when the resulting KER is low; as a result the variation in the signal as a function of τ due to the vibrations will form isolated patches aligned along the zero KER TOF, which we call "islands" (see, for example, Fig. 4). In this paper, we use the TOF axis as a reference for all angles (parallel, perpendicular, etc.), unless indicated otherwise.

C. Experimental results

Figure 3(a) shows I^{2+} data from the (2,0) channel taken with a perpendicular pump pulse and a parallel probe pulse. Since we see "loops," according to the TOF geometry mentioned in Sec. II B, the dissociation is along the TOF axis. Figure 4(a) shows similar data taken with the polarization of the pump and the probe pulses rotated by 90°; the vibrations appear as "islands." The "loops" and the "islands" are representations of the same vibrational motion, since rotating the laser polarization does not change the physical process but only the angle of detection. Moreover, the vibrations with the two polarization configurations have the same period and the same phase within measurement uncertainty, as shown in Fig. 4(b). We integrated the counts in the TOF spectrum over a window containing only the low KER (2,0) dissociation for each delay time [a line out of low KER (2,0) channel; in this work a line out refers to that of the low KER (2,0) channel]. Although these two data sets are taken with different intensity ratios, in Fig. 5 we show that it is the direction of the laser polarization that determines the structure of the data rather than the intensity ratio. Figure 5(a) shows the data taken with the same laser polarization as that in Fig. 4(a), but with a reversed intensity ratio; both data sets show "islands." Similarly, as shown in Fig. 5(b), comparing with the data in Fig. 3(a), reversing the intensity ratio does not change the data structure. With this consistency, our experimental results show that a perpendicular pump pulse results in parallel dissociation, while a parallel pump pulse results in perpendicular dissociation. The role that the polarization of the probe pulse plays is discussed in Sec. IV. In that section, we will also argue that this relationship shows that ionization into the excited state $I_2^+A^2\Pi_{u,3/2}$ is stronger when the electric field of the laser is perpendicular to the molecular axis, compared to when it is parallel to the molecular axis, which is, of course, opposite to ionization to the ground state.

The advantage of setting the polarization of the pump and probe pulses perpendicular to each other is that it provides an almost background free zone in the region of interest in TOF. When the pump pulse is perpendicular, the regular (2,0) channel produced by the pump pulse is completely blocked; when the pump pulse is parallel, its intensity can be chosen low enough to close the (2,0) channel. Also, a single-blue pulse does not produce a zero KER signal. Hence, in either case, the background in the region of lower energy (2,0) channel in TOF is low.

The data set in Fig. 5(a) came from a longer delay scan. The fast Fourier transform (FFT) of its line out shown in Fig. 6 yields a vibrational period of 0.276 ± 0.011 ps. This is close to the period for the ground vibrational state of $I_2^+A^2\Pi_{u,3/2}$ 0.240 ps [1,10]. The longer experimental result is reasonable since the most populated vibration level $\nu=\sim 19$ (from the Frank-Condon factors of transition between the two states) is associated with a lower vibrational frequency or a longer vibrational period than the $\nu=0$ level due to the anharmonicity of the PEC. Furthermore, the assignment to the $I_2^+A^2\Pi_{u,3/2}$ state is confirmed by the simulation results discussed later in this paper. Exclusion of other candidate states is discussed in Sec. IV. The data also show that the vibrational motion fades out after about ~ 11 cycles. The amplitude of the wave-packet motion can decrease for several reasons: (1) The population in the excited state can decay to a lower state. (2) The population in the various levels can lose their coherence

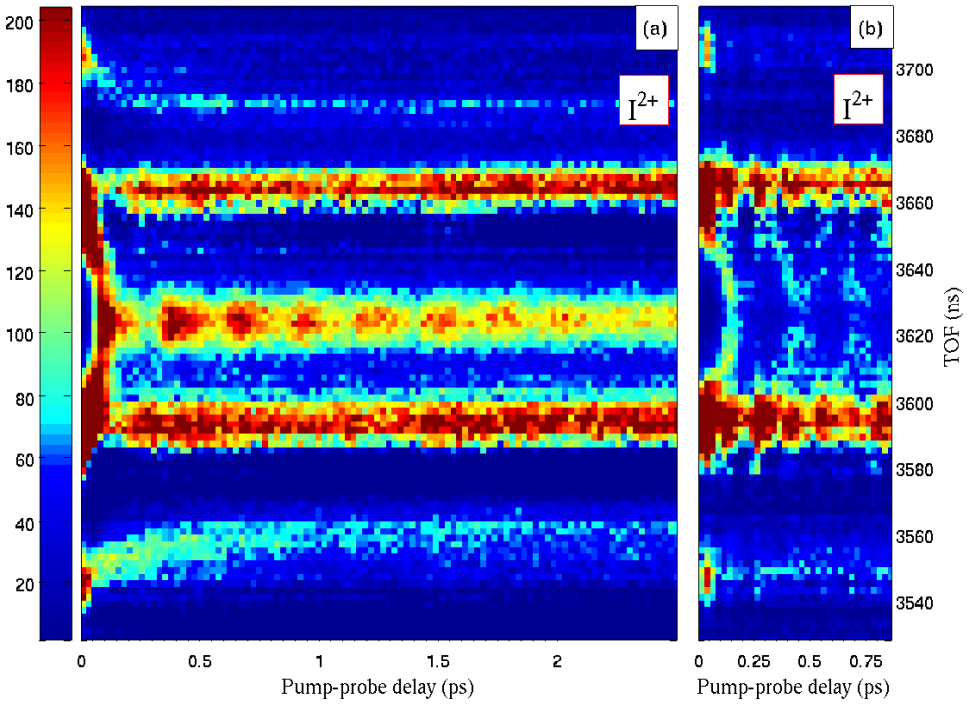

FIG. 5. (Color online) (a) TOF spectrum I^{2+} versus τ with a step size of 0.025 ps. Similar as in Fig. 4(a), the pump pulse is parallel and the probe pulse is perpendicular, but the intensity ratio of the pump and the probe pulses is reversed (2:1). (b) Similar as in Fig. 3(a), the pump is perpendicular and the probe is parallel, but with a reversed pump-probe intensity ratio (1:2).

due to dephasing through collisions, for example. (3) The phase of the vibrational levels evolves coherently in such a way that the wave packet spreads out. We believe the latter possibility is responsible for the reduced amplitude of the oscillations due to agreement with the simulations that will be discussed in Sec. III. However, we loosely refer to this behavior as a "decay" for conciseness throughout the rest of the paper.

Once we have identified the intermediate state $(I_2^+A^2\Pi_{u,3/2})$, the (2,0) curve can be obtained via the vibrational patterns. We convert the TOF signals into KER space with the appropriate Jacobian transformation [Fig. 3(b)]. Data points of the total KER of the (2,0) channel are sampled for the second cycle. We approximate the PEC of $I_2^+A^2\Pi_{u,3/2}$ with a Morse potential [19]. The parameters are obtained from fitting data points sampled from the curve in Ref. [10]:

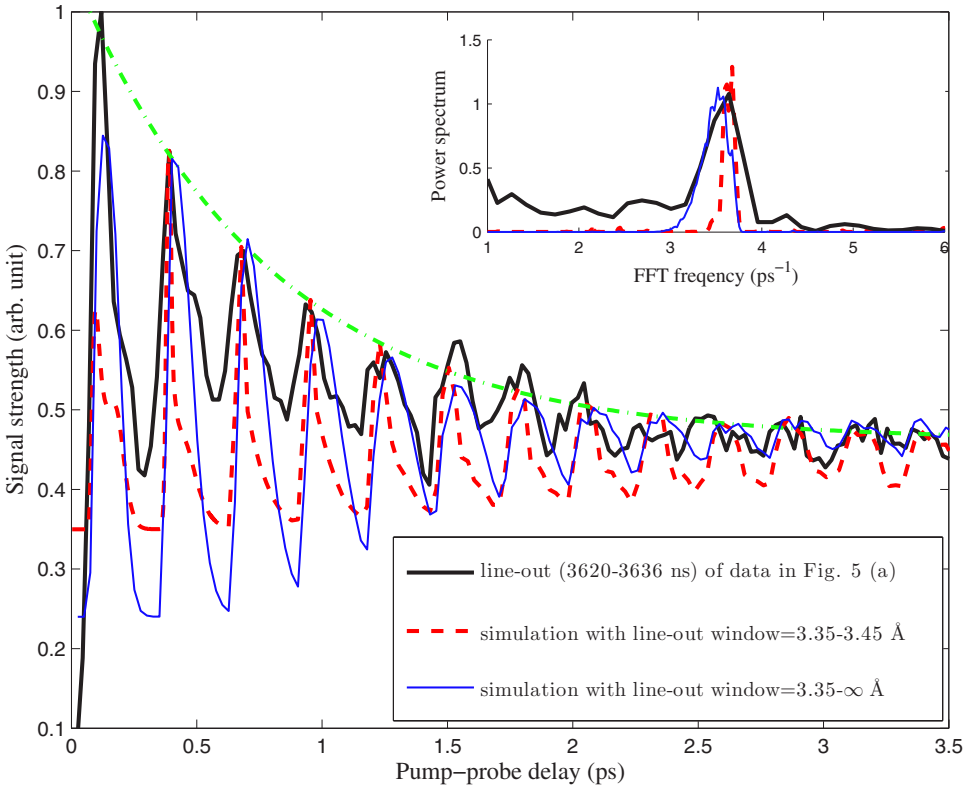

FIG. 6. (Color online) Line out of the data shown in Fig. 5(a); also plotted in this figure: the corresponding line out of the simulation with a window of 3.35–3.45 Å and 3.35 Å to ∞, respectively. Dash-dotted curve: fitted decay profile. Inset: FFT of the corresponding line outs shown in the main panel.

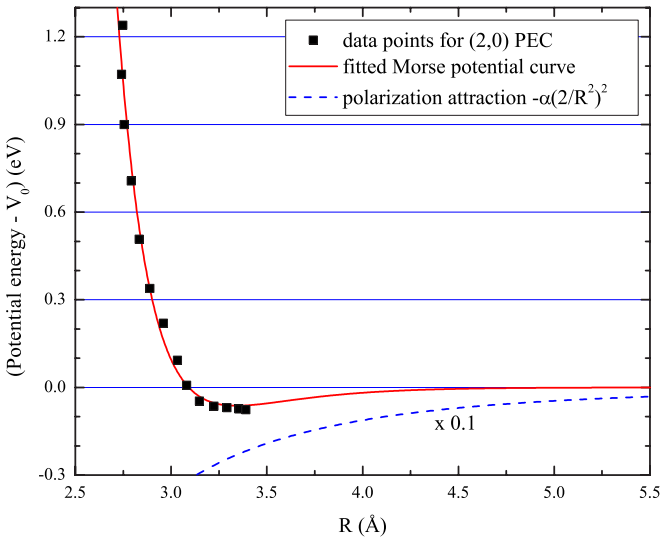

FIG. 7. (Color online) Data points of the (2,0) PEC fitted with Morse potential and the polarization attraction as a function of R. The PEC is relative to the asymptotic limit of the (2,0) curve. Also shown is the polarization attraction of $I^{2+}+I^{0+}$.

$$V(R) = D_e\{1 - \exp[-\beta(R - R_e)]\}^2 + V_0,$$

$$D_e^A = 1.26 \text{ eV}, \quad R_e^A = 2.98 \text{ Å}, \quad \beta^A = 1.31 \text{ Å}^{-1},$$

$$V_0^A = 10.73 \text{ eV}. \tag{1}$$

The parameter V_0^A is chosen so that the PEC is relative to the zero energy of the ground state of I_2 [11].

The initial energy level of the wave packet in the $I_2^+A^2\Pi_{u,3/2}$ state used to obtain the (2,0) curve is found by classical projection of the ground state wave function of I_2 onto the $I_2^+A^2\Pi_{u,3/2}$ curve. With this initial energy of the wave packet, we calculate the KER that is gained from the intermediate $I_2^+A^2\Pi_{u,3/2}$ state. The potential energy for the (2,0) curve is obtained by subtracting the KER mentioned above from the total KER of the (2,0) channel at each R sampled. As shown in Fig. 7, we are able to obtain data for the (2,0) curve up to ~3.4 Å where the KER approaches zero. We fit these data with another Morse potential [Eq. (1)] and find the following values:

$$D_e^{(2,0)} = 0.06 \pm 0.03 \text{ eV}, \quad R_e^{(2,0)} = 3.34 \pm 0.05 \text{ Å},$$

$$\beta^{(2,0)} = 2.8 \pm 0.4 \text{ Å}^{-1}, \quad V_0^{(2,0)} = 31.06 \pm 0.03 \text{ eV}.$$

Again, $V_0^{(2,0)}$ is chosen to make the (2,0) PEC relative to the minimum of the potential energy of the I_2 ground state [11].

Finally, the data in Fig. 4(a) also show the ionization of the dissociating (2,0) channel to the (2,1) channel as a function of τ. These data form smooth curves that we call "tracks." Similar data were used in Ref. [14] to study dissociation channels of I_2^{2+}. We use the (2,0) PEC obtained above and a Coulomb potential with a screening factor of 0.88 for the (2,1) curve to simulate this ionization track as shown in this panel (dashed line). The screening factor is obtained from the same data using the same method as Ref. [14]. The consistency between the data and the simulation further confirms the validity of the (2,0) PEC obtained in our current work.

Since we observed the ionization from the $I_2^+A^2\Pi_{u,3/2}$ state to the (2,0) state, there may also be ions ending up on the $I^+ + I^+$ (1,1) curve that is below the (2,0) curve. However, we do not see comparable vibrations in the (1,1) channel. Based on the (2,0) PEC, in the range of the vibrations [R = ~2.67 – ~3.50 Å, the two classical turning points (TPs)], the (2,0) curve cannot be treated as flat and is in fact significantly steeper than the (1,1) curve that we approximate with a screened Coulomb potential (see Fig. 1). Therefore, in this range of R, the ions gain more KER through the (2,0) channel than through the (1,1) channel leading to a larger variation in TOF in the (2,0) channel (~21 ns) than in the (1,1) channel (~13 ns). Moreover, the (2,0) channel has a more narrow TOF distribution [full width at half maximum (FWHM) = ~12 ns] than the (1,1) channel (FWHM = ~30 ns). The visibility of the vibrations will be proportional to the ratio of the variation in TOF to the width of the channel and, therefore, will be much greater for the (2,0) channel than for the (1,1) channel. Of course, ionization of the $I_2^+A^2\Pi_{u,3/2}$ state may selectively populate the (2,0) curve. This question is beyond the scope of this work, although will be the subject of further study.

III. SIMULATION RESULTS

We solved the time-dependent Schrödinger equation to simulate the evolution of the wave packet in the $I_2^+A^2\Pi_{u,3/2}$ state. For I_2 at room temperature (295 K) as it is in our current work, populations for the first three vibrational levels of the I_2 ground electronic state (ν=0,1,2) are 60%, 21%, 7.4%, respectively, according to the Boltzmann distribution. We directly project these three states onto the $I_2^+A^2\Pi_{u,3/2}$ state to start the simulation. This direct projection is valid for ionization of heavy molecules like I_2 by a ~40 fs short pulse. Also, it predicts a phase of the vibrations consistent with the data. Since I_2 in the ground electronic state has an equilibrium internuclear separation R_e (2.67 Å) that is smaller than that of $I_2^+A^2\Pi_{u,3/2}$ (2.98 Å) [1,20], the direct projection will start the vibration at the inner TP and the wave packet will reach the outer TP at one half period later. In terms of KER, initially the KER would be a maximum and reach a minimum a half cycle later as seen in the data. The final population of $I_2^+A^2\Pi_{u,3/2}$ is calculated by adding up the three resultant populations (starting on ν=0,1,2) incoherently using the normalized population of each initial state as their weights. The initial wave functions of the ground state of I_2 are calculated using a separate program [21]. The PEC of $I_2^+A^2\Pi_{u,3/2}$ used is the same as mentioned in Sec. II C.

Figure 8(a) shows the motion of the wave packet as a function of time. The wave packet stays localized for the first 2 cycles and spreads out as the evolution time increases. However, the eigenfunctions regain their in-phase status some time later leading to a full revival of the wave packet as shown in Fig. 8(b). As also shown in the simulation, the wave packet does not oscillate uniformly. There is an asymmetry of the wave-packet localization between the first half

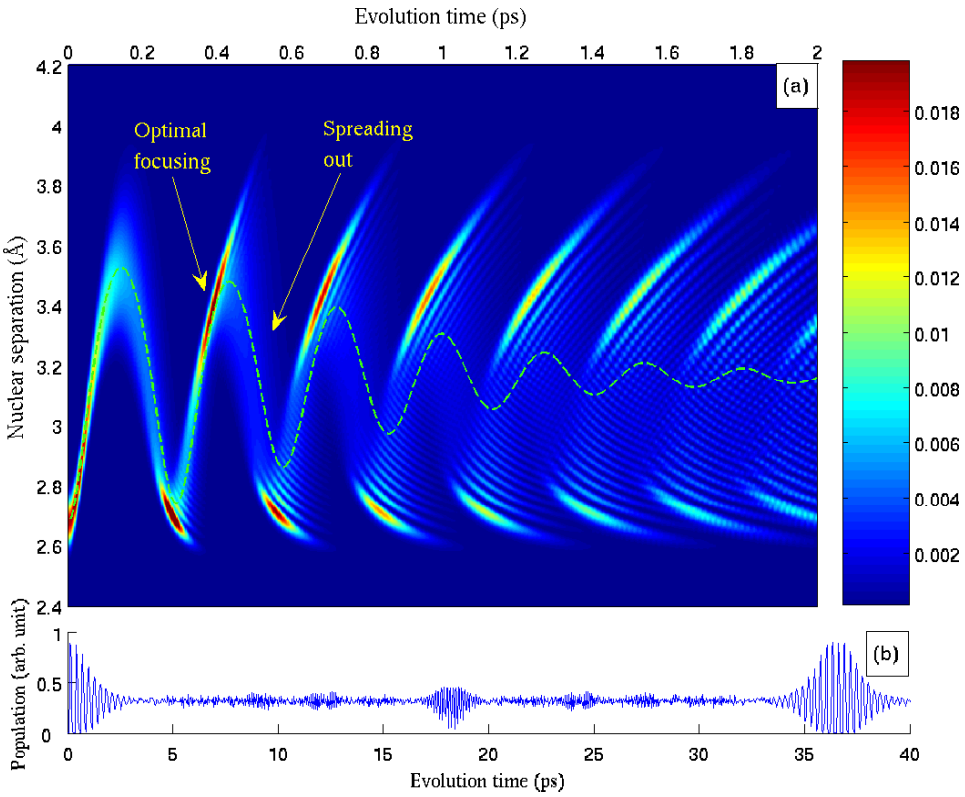

FIG. 8. (Color online) Simulation of the wave-packet evolution. (a) Two-dimensional (2D) plot of the evolution of the wave packet. The horizontal axis (top axis) is the evolution time which corresponds to the pump-probe delay (τ) in the experiments. The vertical axis is the internuclear separation R. Dashed line: expectation value of R that is used in the simulation of the "loops" (see text). (b) (bottom axis) Line out of simulation of the wave-packet evolution with a window of 3.35–3.45 Å. Note, for (b), only the $\nu=0$ state of I_2 was included.

cycle (i.e., when the wave packet moves towards the outer TP) and the second half cycle (i.e., when the wave packet moves back towards the inner TP): a more compact wave packet is seen in the first half cycle than in the second half cycle. This asymmetry is indeed shown in our data: with stronger focusing of the wave packet, a more intense signal is detected in the first half cycle than that in the second half cycle where the wave packet is more spread out. Moreover, clearly shown in the simulation, in the second full cycle of the vibration, an optimal focusing occurs only in the first half cycle and at a time (t=0.387 ps, R=3.4 Å) before the wave packet reaches the outer TP (R=3.5 Å). This is also seen in our data [see Fig. 3(a), indicated by arrows], where this "early" maximum focusing occurs at a time $\tau=\sim$0.390 ps consistent with the calculation results.

To further compare the experimental and simulation results, we use a flat-top window centered at R of the optimal focusing (R=3.35–3.45 Å) to produce a line out of the simulation. The FFT of the line out (see inset in Fig. 6) gives a vibrational period of 0.275±0.004 ps, which is the same within uncertainty as that from the data (0.276±0.011 ps). The decay of the vibrations also shows good consistency between the data and the simulation. We fit the decay profile using a first-order exponential function $A\exp(-t/\tau_0)+y_0$ and the fitted decay time parameter τ_0 is 0.78±0.02 ps (dash-dotted curve in the main panel of Fig. 6). The consistency of the data with the calculations in vibrational period, decay rate, and timing of wave packet focusing verifies that the parent state of the vibrations observed in the experiments is $I_2^+A^2\Pi_{u,3/2}$.

IV. DISCUSSION

Although the results of the simulation match the experimental results well, there are still several other states that need to be considered. However, they can all be excluded as follows. First, there are two states with similar vibrational periods as that in the data: the $B^3\Pi_u$ state of I_2 and the $a^4\Sigma_u^-$ state of I_2^+. Their $\nu=0$ vibrational periods are 265 fs and 260 fs, respectively (see Table I). However, for the former, since the blue light has a single-photon energy of 3.1 eV that is beyond the 2 eV one-photon excitation energy for the B state, the direct excitation to the B state is not likely with blue photons. As to the latter, the transition is spin-forbidden [10]. Second, the lower states $X^2\Pi_{g,3/2}$ and $X^2\Pi_{g,1/2}$ of I_2^+ are probably also populated by the pump pulse. However, with

TABLE I. Properties of electronic states of I_2 and I_2^+ (experimental results).

	State	ω_e (cm^{-1}) [period (fs)]	T_e (eV)[a]	Configuration
I_2	$X^1\Sigma_g^+$	214.5 [155]	0	$\sigma_g^2\pi_u^4\pi_g^4\sigma_u^0$
	$B^3\Pi_u$	125.7 [265]	1.96	$\sigma_g^2\pi_u^4\pi_g^3\sigma_u^1$
I_2^+	$X^2\Pi_{g,3/2}$	240±1 [139±0.6]	9.31	$\sigma_g^2\pi_u^4\pi_g^3\sigma_u^0$
	$X^2\Pi_{g,1/2}$	229±2 [146±1]	9.95	$\sigma_g^2\pi_u^4\pi_g^3\sigma_u^0$
	$A^2\Pi_{u,3/2}$	138±2 [242±4]	10.96	$\sigma_g^2\pi_u^3\pi_g^4\sigma_u^0$
	$a^4\Sigma_u^-$	128±2 [260±4]	10.66	$\sigma_g^2\pi_u^4\pi_g^2\sigma_u^1$

[a]References [1,2,10,19,22–25]. Vertical ionization energy at R_e of the ground state of I_2.

TABLE II. Theoretical vibrational frequencies of the $A^2\Pi_{u,3/2}$ and $A^2\Pi_{u,1/2}$ states of I_2^+.

	$A^2\Pi_{u,3/2}$	$A^2\Pi_{u,1/2}$
ω_e (cm^{-1})	132 [252][a]	112 [298][a]
[period (fs)]	133 [251][b]	117 [285][b]

[a]Reference [26].
[b]Reference [1].

vibrational periods of 139 fs and 146 fs, even with higher vibrational states populated, the resulting vibrational periods still do not match the value obtained in our experiments. For the $A^2\Pi_{u,1/2}$ state, no experimental results for the vibrational frequency are available in the literature. However, theoretical calculations in which the vibrational frequency of the $I_2^+A^2\Pi_{u,3/2}$ state is consistent with the experimental results predict a vibrational period for the $A^2\Pi_{u,1/2}$ state that is 45 fs (average) above that for the $I_2^+A^2\Pi_{u,3/2}$ state (see Table II). Consequently, this $j=\frac{1}{2}$ state is also excluded. Therefore, we conclude that the state responsible for the vibrations observed in this work is $I_2^+A^2\Pi_{u,3/2}$.

The observation of the excitation of the $I_2^+A^2\Pi_{u,3/2}$ state with the pump pulse reveals that an ultrashort laser pulse can do more than simply remove the least bound electron. It can leave the resulting molecular ion in a mixture of ground and excited electronic states. For the excitation of the $I_2^+A^2\Pi_{u,3/2}$ state, there are two paths: either $I_2 \rightarrow I_2^+ X^2\Pi_{g,3/2} \rightarrow$ (resonant excitation) $I_2^+A^2\Pi_{u,3/2}$, or $I_2 \rightarrow I_2^+A^2\Pi_{u,3/2}$. Because of the ~1.65 eV gap in ionization energy (see Table I and Fig. 1), the $I_2^+A^2\Pi_{u,3/2}$ state is off resonant with the $X^2\Pi_{g,3/2}$ state with a blue photon (3.1 eV). So the resonant excitation is not likely. Recollision is also not a likely mechanism for the excitation, because the recollision theory is based on a tunneling model and our experimental condition gives a value for the Keldysh parameter $\gamma=2.5$–3.4 indicating that we are in the multiphoton ionization regime. Hence, we conclude that the $I_2^+A^2\Pi_{u,3/2}$ state observed in this work is populated directly from the ground electronic state of I_2. Looking at the molecular configurations in Table I, we see that in this case the $I_2^+A^2\Pi_{u,3/2}$ state can be obtained from the ground state by the removal of a π_u electron. In other words, our results show that, as in N_2 [8], a single laser pulse can remove an electron from an inner orbital of I_2 without stripping the electron in the highest occupied molecular orbital (HOMO). This possibility of inner-orbital ionization needs to be taken into account in quantum tomography experiments that use high-harmonic generation to image molecular orbitals.

The frequency analysis approach introduced in this work makes it possible to identify bound electronically excited molecular states in TOF spectroscopy. It should work well for states with distinguishable vibrational frequencies. Since the simulation results explain the data well in both the motion and the localization of the wave packet, this approach should be a robust method to investigate excited-state potential wells. In particular, the full revival time is sensitive to the shape of the potential curve. In the simulation that has been presented in Sec. III, we use $\beta=1.31$ $Å^{-1}$ for the Morse potential [Eq. (1)] which corresponds to a $\nu=0$ vibrational frequency of 136 cm^{-1}. The simulation result gives a revival time of 36.6 ps. We decrease the frequency mentioned above by 10 cm^{-1} to 126 cm^{-1} and use the corresponding curve in the calculation. The resulting revival time increases to 40 ps. The 3.4 ps shift is dramatic in pump-probe spectroscopy that has a 0.5 fs resolution. Consequently, measuring the revival time can provide even more accurate data to test bound potential curves, although this may require a cold sample of molecules.

The simulations show a full picture of the wave-packet evolution, and the results provide a good interpretation of the data. However, in experiments the observations are constrained by the probing schemes. Simulating the probing method in theoretical calculations is crucial for representing observable results; conversely, the discrepancy between experimental and theoretical results may give information about the probing process. In this work, using a flat-top window in the line out is a coarse approximation that assumes only the wave packet itself in that window determines the signal strength. Actually, the discrepancy between data and simulations though small, implies other important physics in the process that needs exploration. For example, as shown in Fig. 3(b), the "loops" do not decay as predicted by the simulation when the expectation values of R are used to determine the KER [dashed line in Fig. 8(a)]. That may be due to the R dependence of the ionization rate. For example, if the ionization rate maximizes at an R larger than the outer TP, the apparent motion of the wave packet will be biased to larger values of R, resulting in smaller KER than predicted. In the tunneling model of diatomic-molecule ionization, a critical R (R_c) of about ~5 Å is theoretically predicted and experimentally verified (with a long wavelength of ~790 nm) for molecules in their ground electronic states [27–29]. This R_c is insensitive to the number of electrons in the molecule and the charge state, but may be affected by the wavelength of the laser since a nonadiabacity condition is required, i.e., the electron at one nucleus does not tunnel back to the lower-lying well within half an optical cycle [30]. If we assume this to be true for an excited state of I_2^+, we should be able to extend our integration window from $R=3.35$ Å to infinity, since R_c is significantly greater than the outer TP. However, this integration window does not lead to good agreement with the data. Comparing the line out using this semi-infinite window with a square function window, as shown in Fig. 6, the former does not fit the data as well as the latter in two aspects: first, the line out of the former yields a vibrational period of 285 fs which is slightly longer (see the inset); second, it lacks the asymmetry characteristic of a single peak in the line out (a steep increase on the first half cycle and a more gradual decrease on the second half cycle). Although, the square function used for a finite window is only a rough approximation, its better agreement with the data than the semi-infinite one shows that for bound excited electronic state $I_2^+A^2\Pi_{u,3/2}$ ionization as a function of R is different from the ground electronic state, probably with a smaller R_c. This is consistent with previous observations that ionization from the ground state to charge asymmetric channels occurs at smaller R than symmetric channels [4]. This result raises questions concerning the nonadiabacity condition provided by blue photons and the charge resonant states for an electronically excited molecular ion.

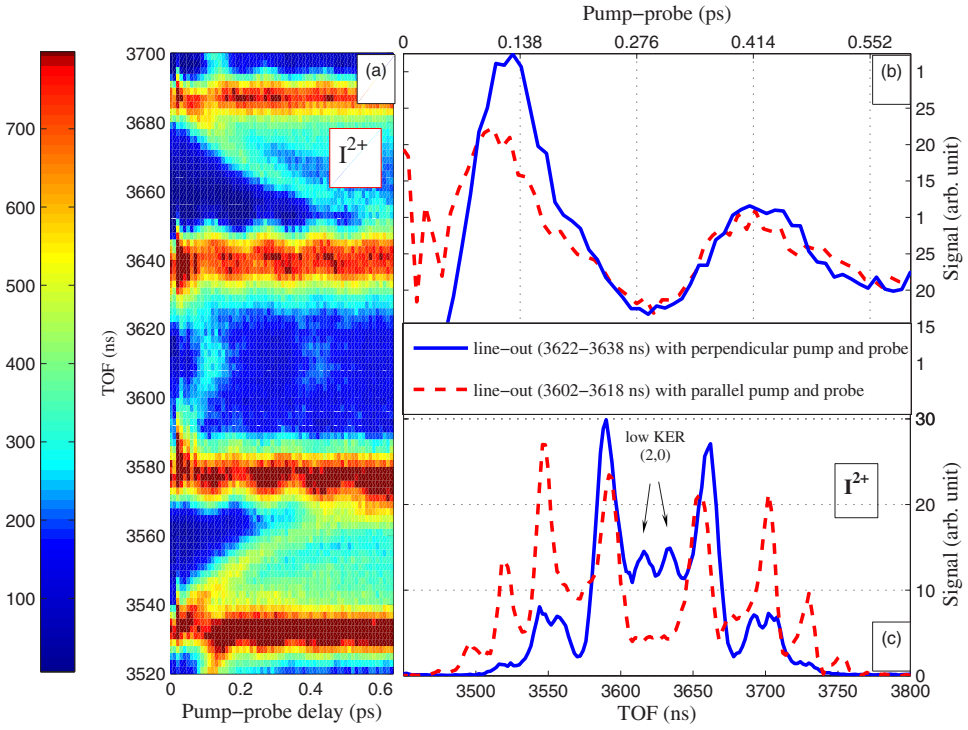

FIG. 9. (Color online) (a) TOF spectrum of I^{2+} versus τ with polarization of both the pump and the probe pulse parallel to the TOF axis. The intensity ratio of the pump and the probe pulse is 1:2. The vibrations appear as weak "loops." (b) Line outs of two data sets. Solid line: data taken with perpendicular pump and parallel probes shown in Fig. 3. Dashed line: data in (a). (c) Integrated TOF signals over the delay span of the second full cycle (τ=0.280–0.550 ps). The spectra are rescaled so that the signals produced by the pump pulses are equivalent in the two data sets.

As discussed in Sec. II C, the dissociation occurs in a direction that is perpendicular to the electric field of the pump pulse. These results further reveal a polarization dependence of the ionization of I_2 to the $I_2^+A^2\Pi_{u,3/2}$ state. Since a short femtosecond pulse at moderate intensity is not efficient in aligning I_2 [15,16,31], it is reasonable to assume that a femtosecond pulse used in this work will not affect the orientation of a molecular ion in the $I_2^+A^2\Pi_{u,3/2}$ state either, which has an even larger momentum of inertia due to its larger R_e [1,20]. Therefore, the dissociation direction reflects the orientation of the molecular axis of the ionizing I_2. Consequently, our results show that ionization of I_2 to the $I_2^+A^2\Pi_{u,3/2}$ is stronger with an electric field perpendicular to the molecular axis compared to an electric field parallel to the axis. To further confirm this polarization dependence of the ionization, we show in Fig. 9 the data taken with both the pump and the probe pulses parallel to the TOF axis. In this data as shown in Fig. 9(a), we see weak "loops." They have the same vibrational period and phase as those in the data taken with the pump and probe pulses perpendicular to each other, as shown by the line out in Fig. 9(b). The slight shift in the pulse delay for the first maximum is due to the strong interference of the two pulses near τ=0. As shown in Fig. 9(c), under the same pump strength, with even a relatively stronger probe pulse the parallel configuration produces much weaker vibrations than the perpendicular configuration. The resulting weak vibrations confirm our observation that ionization to the $I_2^+A^2\Pi_{u,3/2}$ state does have a preferential polarization of the electric field, which is perpendicular to the molecular axis as discussed above. The behavior of the molecules or ions in a high laser field is usually related to their internal structure. For a molecular ion to be in the $I_2^+A^2\Pi_{u,3/2}$ state, an electron in the π_u orbital is removed instead of the π_g HOMO [10]. The π_u orbital has a reflection symmetry with respect to the molecular axis. This property may contribute to the polarization dependence of removing an electron from that orbital.

As discussed above, the pump pulse produces ions in the $I_2^+A^2\Pi_{u,3/2}$ state aligned perpendicular to the electric field. Data in Fig. 9 shows that a probe pulse perpendicular to the molecular axes of the ions produces much weaker vibrations in the dissociation channel than a probe pulse parallel to the molecular axes as shown in Figs. 3–5. That means the ionization of $I_2^+A^2\Pi_{u,3/2} \rightarrow (2,0)$ is preferred with the electric field parallel to the molecular axis. Further study of the polarization dependence of the ionization to the (2,0) channel may produce information about the molecular orbital of the (2,0) state and therefore extend our understanding of electronically excited molecular states correlating with charge-asymmetric dissociation limits.

In Sec. II C, we mentioned the (2,0) PEC is steep in the R range probed in this work. Moreover, it drops into a bound region to a depth of 0.06 eV at R=3.34 Å. This is remarkable in that we are not aware of any other vibrationally bound states of diatomic dictations, despite the extensive literature on metastable states of N_2^{2+} [32,33], Cl_2^{2+} [34,35], and I_2^{2+} [36]. However, true binding on the (2,0) curve is not unreasonable, since there is a strong polarization attraction that dominates at long range. In Fig. 7, the dashed line shows the polarization attraction as a function of R, $V(R) = -\alpha(2/R^2)^2$, where α=72 eV Å^4 [14,37,38]. Since there is no Coulomb repulsion between I and I^{2+}, the contribution of this polarization attraction to the potential energy can easily provide sufficient binding character to produce the observed well depth before short-range repulsion takes over.

In our previous work we used the ionization path of $(2,0) \rightarrow (2,1)$ to obtain an approximate PEC of the (2,0) channel [14]. Although it was good as a first attempt, a Coulomb curve which is a long-range approximation is not accurate in short range around R_e. However, potential energy

curves in this short range are important since it is in this range that the direct projection by short laser pulses takes place. Using a well-known curve, we are able to avoid the error due to the uncertainty of the (2,1) curve used to investigate the (2,0) curve.

V. CONCLUSION

In this paper, we present the work of using vibrational wave packets to identify a bound electronically excited state of I_2^+ and using this state to investigate the (2,0) curve in TOF spectroscopy. By studying the vibrational patterns, we are able to extract information of both potential curves involved. A potential well of 0.06 eV is found for the (2,0) PEC. The results provide further evidence of the excitation of molecular ions through inner orbital ionization by strong laser fields. The theoretical calculations further confirm the physical process and together with the experimental results, show the quantum mechanical nature of the wave packet and extend the studies of ionization rate as a function of R. Finally, we see an anomalous polarization dependence of ionization of inner orbital electrons: the ionization is stronger with the electric field perpendicular to the molecular axis. In addition, the ionization of $I_2^+ A^2\Pi_{u,3/2} \rightarrow (2,0)$ is stronger with an electric field along the molecular axis.

Further study of the R dependence and the angular dependence of the ionization rate for excited electronic states is needed. However, this is possible with pump-probe TOF techniques now that we are able to identify the excited electronic states.

ACKNOWLEDGMENTS

We would like to acknowledge support from the NSF under Grant No. PHYS-0244658 and conversations with Tom Weinacht.

[1] W. A. de Jong, L. Visscher, and W. C. Nieuwpoort, J. Chem. Phys. **107**, 9046 (1997).
[2] A. J. Yencha, M. C. Cockett, J. G. Goode, R. J. Donovan, A. Hopkirk, and G. C. King, Chem. Phys. Lett. **229**, 347 (1994).
[3] J. J. Larsen, I. Wendt-Larsen, and H. Stapelfeldt, Phys. Rev. Lett. **83**, 1123 (1999).
[4] G. N. Gibson, M. Li, C. Guo, and J. P. Nibarger, Phys. Rev. A **58**, 4723 (1998).
[5] J. P. Nibarger, M. Li, S. Menon, and G. N. Gibson, Phys. Rev. Lett. **83**, 4975 (1999).
[6] T. J. Dunn, I. A. Walmsley, and S. Mukamel, Phys. Rev. Lett. **74**, 884 (1995).
[7] S. Patchkovskii, Z. Zhao, T. Brabec, and D. M. Villeneuve, Phys. Rev. Lett. **97**, 123003 (2006).
[8] G. N. Gibson, R. R. Freeman, and T. J. McIlrath, Phys. Rev. Lett. **67**, 1230 (1991).
[9] J. Che, J. L. Krause, M. Messina, K. R. Wilson, and Y. Ya, J. Phys. Chem. **99**, 14949 (1995).
[10] M. C. R. Cockett, R. J. Donovan, and K. P. Lawley, J. Chem. Phys. **105**, 3347 (1996).
[11] In both cases [the A state of I_2^+ and the (2,0) state], V_0 is determined by the dissociation energy of the I_2 X state D_e^X and the state being defined. Also, the ionization potentials I_p of the separated atoms must be added: $V_0^A = D_e^X + I_p(I) - D_e^A$; $V_0^{(2,0)} = D_e^X + I_p(I) + I_p(I^+) - D_e^{(2,0)}$. Atomic ionization potentials are from http://physics.nist.gov/PhysRefData/Handbook/Tables/iodinetable1.htm
[12] E. Skovsen, M. Machholm, T. Ejdrup, J. Thøgersen, and H. Stapelfeldt, Phys. Rev. Lett. **89**, 133004 (2002).
[13] T. Ergler, A. Rudenko, B. Feuerstein, K. Zrost, C. D. Schröter, R. Moshammer, and J. Ullrich, Phys. Rev. Lett. **95**, 093001 (2005).
[14] G. N. Gibson, R. N. Coffee, and L. Fang, Phys. Rev. A **73**, 023418 (2005).
[15] H. Stapelfeldt and T. Seideman, Rev. Mod. Phys. **75**, 543 (2003).
[16] C. Ellert and P. B. Corkum, Phys. Rev. A **59**, R3170 (1999).
[17] M. Li and G. N. Gibson, J. Opt. Soc. Am. B **15**, 092404 (1998).
[18] J. P. Nibarger, S. V. Menon, and G. N. Gibson, Phys. Rev. A **63**, 053406 (2001).
[19] M. C. R. Cockett, J. G. Goode, K. P. Lawley, and R. J. Donovan, J. Chem. Phys. **102**, 5226 (1995).
[20] M. S. Mason and R. P. Tuckett, Chem. Phys. Lett. **160**, 575 (1989).
[21] R. J. LeRoy, University of Waterloo, Level 7.4, A Computer Program for Solving the Radial Schrödinger Equation for Bound and Quasibound Levels.
[22] C. J. Bardeen, J. Che, K. R. Wilson, V. V. Yakovlev, V. A. Apkarian, C. C. Martens, R. Zadoyan, B. Kohler, and M. Messina, J. Chem. Phys. **106**, 8486 (1997).
[23] T. Ishiwata, H. Ohtoshi, M. Sakaki, and I. Tanaka, J. Chem. Phys. **80**, 1411 (1984).
[24] J. Tellinghuisen, J. Chem. Phys. **58**, 2821 (1973).
[25] F. Martin, R. Bacis, S. Churassy, and J. Vergès, J. Mol. Spectrosc. **116**, 71 (1986).
[26] Q. Li and K. Balasubramanian, J. Mol. Spectrosc. **138**, 162 (1989).
[27] G. N. Gibson, M. Li, C. Guo, and J. Neira, Phys. Rev. Lett. **79**, 2022 (1997).
[28] T. Zuo and A. D. Bandrauk, Phys. Rev. A **52**, R2511 (1995).
[29] E. Constant, H. Stapelfeldt, and P. B. Corkum, Phys. Rev. Lett. **76**, 4140 (1996).
[30] S. Chelkowski, T. Zuo, O. Atabek, and A. D. Bandrauk, Phys. Rev. A **52**, 2977 (1995).
[31] F. Rosca-Pruna and M. J. J. Vrakking, Phys. Rev. Lett. **87**, 153902 (2001).
[32] W. T. Hill III, J. Zhu, D. L. Hatten, Y. Cui, J. Goldhar, and S. Yang, Phys. Rev. Lett. **69**, 2646 (1992).
[33] H. R. Koslowski, H. Lebius, V. Staemmler, R. Fink, K. Wiesemann, and B. A. Huber, J. Phys. B **24**, 5023 (1991).
[34] J. S. Wright, G. A. DiLabio, D. R. Matusek, P. B. Corkum, M. Y. Ivanov, C. Ellert, R. J. Buenker, A. B. Alekseyev, and G.

Hirsch, Phys. Rev. A **59**, 4512 (1999).
[35] J. H. Beynon, R. M. Caprioli, and J. W. Richardson, J. Am. Chem. Soc. **93**, 1852 (1971).
[36] J. Juul, L. N. Bjerre, M. Machholm, S. R. Keiding, and H. Stapelfeldt, J. Chem. Phys. **109**, 8857 (1998).
[37] K. Drühl, J. Chem. Phys. **75**, 5579 (1981).
[38] J. Vigue, M. Saute, and M. Aubert-Frécon, J. Chem. Phys. **78**, 4544 (1983).